Hindawi
Mathematical Problems in Engineering
Volume 2021, Article ID 8917134, 9 pages
https://doi.org/10.1155/2021/8917134

Research Article

Experimental Application of Robust and Converse Dynamic Control for Rotary Flexible Joint Manipulator System

Ahmed IM. Iskanderani [1] **and Ibrahim M. Mehedi** [2]

[1]*Department of Electrical and Computer Engineering (ECE), King Abdulaziz University, Jeddah 21589, Saudi Arabia*
[2]*Department of Electrical and Computer Engineering (ECE), Center of Excellence in Intelligent Engineering Systems (CEIES), King Abdulaziz University, Jeddah 21589, Saudi Arabia*

Correspondence should be addressed to Ibrahim M. Mehedi; imehedi@kau.edu.sa

Received 1 June 2021; Revised 10 June 2021; Accepted 14 June 2021; Published 23 June 2021

Academic Editor: Dr. Dilbag Singh

Performance evaluation of trajectory tracking for a rotary flexible joint system is demonstrated in this paper. The robust and converse dynamic (RCD) technique is proposed and implemented for this evaluation. This control methodology is of the left inversion type, i.e., the control inputs are obtained by means of plant output error feedback. RCD control encompasses the baseline inverse (BI) control and sliding mode control-based discontinuous control element. The baseline inverse controller enforces the prescribed servo (virtual) constraints that represent the control objectives. The control objectives of the baseline inverse controller are enclosed in the form of servo (virtual) constraints which are inverted using Moore–Penrose Generalized Inverse (MPGI) to solve for the baseline control law. To boost the robust attributes against parametric uncertainties and disturbances, a discontinuous control function is augmented with baseline controller such that semiglobal practical stability is guaranteed in the sense of Lyapunov. To exhibit the effectiveness of RCD control in terms of tracking performance, computer simulations are conducted in Simulink/Matlab environment. Furthermore, the practical implementation is also investigated through a real-time experiment on Quanser's rotary flexible joint manipulator system. The experimental results obtained by RCD are compared to the conventional sliding mode and fractional-order control techniques.

1. Introduction

Flexibility influences the performance of the system more than rigidity. A flexible joint manipulator is subject to nonlinearity and uncertainty, particularly mismatched uncertainty.. Therefore, it is necessary to focus on joint flexibility while performing modeling and controller design to obtain satisfactory performance. This flexible joint manipulator is used as a robotic arm for industrial automation. This type of industrial robot accelerates the speed of production and increases accuracy and precision. Flexible joint-based robotic arms have some other applications, such as in space operations. Besides these, flexible joint manipulator can act as an inspector, capable to perform maintenance work, and also can refuel the vehicle. The manipulator can also be a useful tool for the planetary surface explorer to investigate the natural valuable resources during space missions. However, precise robot manipulators with flexible joints can perform several risky operations even during natural disasters.

The main challenge for a rotary flexible joint is to develop a suitable control mechanism that will allow it to perform at a high level. Specifically, the rotary arm's displacement and the arm's flexibility are the two important issues in this system. By controlling the rotary arm, one minimizes the vibration of the flexible joint while maintaining the desired position. In order to enhance the efficiency of rotary flexible joint-based robotic arms, the limit of actuator saturation should be maintained. The size and mass of a powerful motor prevent it from being used. Additionally, a motor that is powerful will consume more power.

The flexible joint control system has been the subject of various investigations. As a part of the design, the arm tip was set to align with the reference direction so as to reduce vibration. Using quadratic d-stability design, we controlled a flexible robotic arm that showed non-minimum phase behaviour [1]. Pole placement-based controller was considered to produce the desired performance by testing it on the physical system in this investigation. It was controlled with a double loop feedback closed path, with the inner loop controlling the position of the motor and the outer loop controlling the arm's movements [2, 3]. Using linear matrix inequalities, a state feedback method was used to design a fuzzy controller for this complex flexible arm problem [4]. Again, a feed-forward closed-loop controller was developed proposing a robust backstepping algorithm for this problem [5]. A Lyapunov approach was used for this investigation against mismatch uncertainty to design a robust virtual controller. A PID control technique is used to justify this backstepping algorithm. The tracking performance of a robotic flexible joint was evaluated using tracking operator design technique in [6]. To minimize the resonating of flexible arms and to control the deflection of their tips, a hybrid controller was also designed that incorporated a double feedback system [7]. Robotic manipulators have also been designed to employ an integral resonant control method (IRC) to reduce resonance [8]. Besides all of these, nonlinear control approach was presented by using observer-based fuzzy algorithm and adaptive technique to control a flexible joint system [9, 10]. The backstepping method was used to construct a state transformation of a flexible joint manipulator system in order to introduce robust adaptive control [11]. Although the designed controller did not satisfy the performance due to insufficient actuators, a fractional-order control is another well-known control tool to regulate such complex robotic systems. In addition to controlling these kinds of systems, they can also be used to control a variety of physical systems, as found in [12–16]. Specifically, a fractional-order integral controller was designed and implemented for a rotary flexible joint testbed [17]. The experimental performances obtained by implementing this fractional-order controller (FOC) are well compared in this current manuscript in Section 5.2. The comparisons are mainly shown with respect to the proposed robust and converse dynamic control (RCD) scheme, which is the main focus of this investigation. Fuzzy systems and neuronal networks are also implemented for complicated models that have strong nonlinearities, which are smart controls found in the literature [18–21].

In order to introduce the RCD control scheme, the authors studied different approaches of general dynamic conversion schemes. For example, the literature shows a constraint-based approach to solve many engineering problems that encapsulates the control objectives in the form of constraint differential equation [22]. To fulfill the control objectives, the constraint dynamics along the trajectories of the dynamical system are inverted by engaging Moore–Penrose Generalized Inverse (MPGI) to establish the control law [22]. The conventional BI strategy explicitly depends on the modeled dynamics; therefore, it lacks robustness to handle system uncertainties and nonlinearities.

Robust and converse dynamic (RCD) control is implemented in this work to solve the control problem of a rotary flexible joint (RFJ) manipulator system that is operating in uncertain parametric control parameters. Using the RCD control technique, both numerically and experimentally, this is the first study to systematically investigate the control of a flexible joint manipulator. Using the sliding mode control (SMC) theory that has been proven extremely robust, we have proposed a combination of baseline controllers and a discontinuous controller [22]. The integration of discontinuous control term makes the control strategy capable to handle the variations in the plant dynamics very effectively while suppressing the strong joint flexibility. As part of the robustness analysis, we present the comprehensive and strict stability analysis of the overall control structure in terms of Lyapunov, so that the tracking performance is guaranteed to be asymptotically stable on the semiglobal scale [23, 24]. A numerical simulation and real-time experiment were conducted using Quanser's RFJ manipulator system to verify the performance of the intended controller. Additionally, the performance comparison of RCD control with the conventional SMC and fractional-order controller (FOC) is demonstrated experimentally to validate the robust capabilities.

The rest of the paper is organized as follows. Section 2 explains the mathematical modeling of the RFJ manipulator system. Section 3 provides comprehensive information on RCD control design. Section 4 presents the semiglobal asymptotic stability analysis of the proposed control strategy in terms of Lyapunov. Section 5 presents an experimental analysis and simulation of RCD control and its comparison with a SMC controller. Section 6 gives the conclusion.

2. Rotary Flexible Joint (RFJ)

Rotary flexible joints (RFJs) are systems developed by Quanser [25]. The robotic engineering field uses this tool to analyze vibrations and perform resonance experiments. A typical RFJ experimental platform is introduced here to demonstrate the behaviour of robotic flexible joint arm. When manipulating the link with a manipulator of this type, it is possible that the natural frequency may be excited, which may accelerate the maneuver. Nevertheless, it takes longer than the desired duration for the vibration to decay naturally.

2.1. Platform Presentation. As seen in Figure 1, the physical model of the rotary flexible joints is shown. On the rotary platform, there are two arms, a long arm and a short arm. A 29.8 cm-long long arm, connected with a double spring pivot system, holds the short arm, which is mounted on top of the

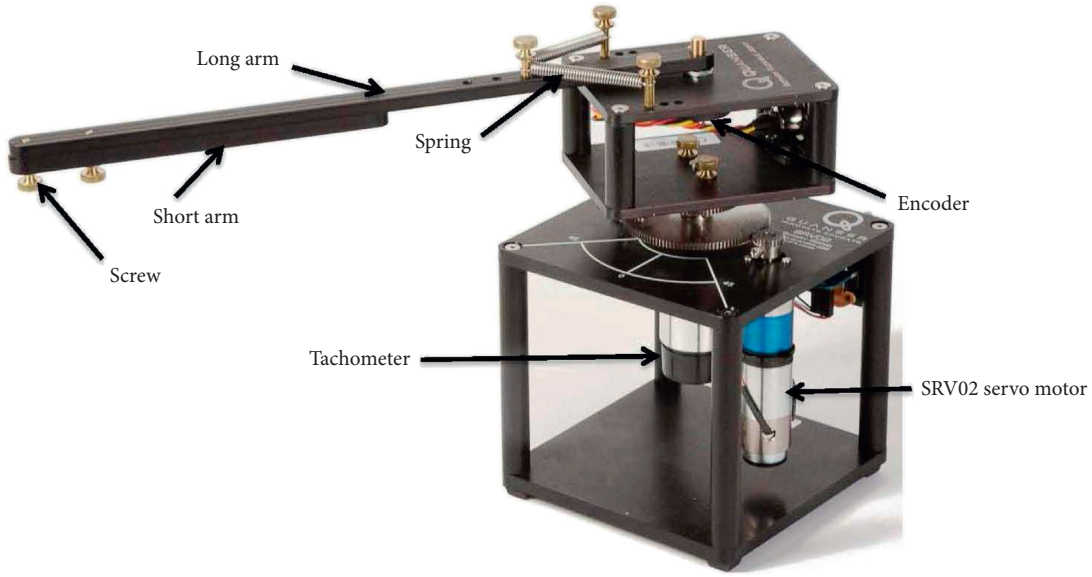

Figure 1: Rotary flexible joint platform.

long arm with two screws. To increase vibration effects of the flexible joint, the short arm can be placed on the long arm differently depending on where it is placed on the long arm. Quanser provided a servo motor base (SRV02) to serve as the base for a spring connection that creates the flexible joint for the rotary arm. This motor is really a complete system, which includes gears, a tachometer, potentiometer, encoders, and a DC motor. By measuring angular displacement of the rotary arm with a tachometer and the orientation of the load gear with a potentiometer, the angular velocity of the rotary arm can be found. The servo load shaft angle and joint rotation angle are measured by two encoders.

2.2. Mathematical Model. See [25] for a schematic of the RFJ system shown in Figure 2. In the RFJ system, the symbol θ represents the angular displacement of rotary arm, whereas α is the vibration angle of the flexible joint. As the arm moves along the horizontal plane, the vibration angle tends to increase. There are two variables, m_1 and m_2 and l_1 and l_2, which, respectively, represent the mass and the length of the long and short arms. Short arm distance is determined by d_{12}.

In [25], a rotary flexible joint system dynamic model is presented in the form of differential equations. The system dynamics are given as follows:

$$\begin{aligned} J_{\text{eq}}\ddot{\theta} + J_l(\ddot{\theta} + \ddot{\alpha}) &= \tau - B_{\text{eq}}\dot{\theta}, \\ J_l(\ddot{\theta} + \ddot{\alpha}) + K_s\alpha &= 0. \end{aligned} \tag{1}$$

In this dynamic model, τ is the output torque and J_l is the inertia of the arm, whereas J_{eq} is the equivalent moment of inertia of servo motor [26]. The servo system realizes some equivalent damping term denoted by B_{eq}, whereas B_l and K_s represent the viscous damping force coefficient acting on the link and linear spring stiffness, respectively. The expression

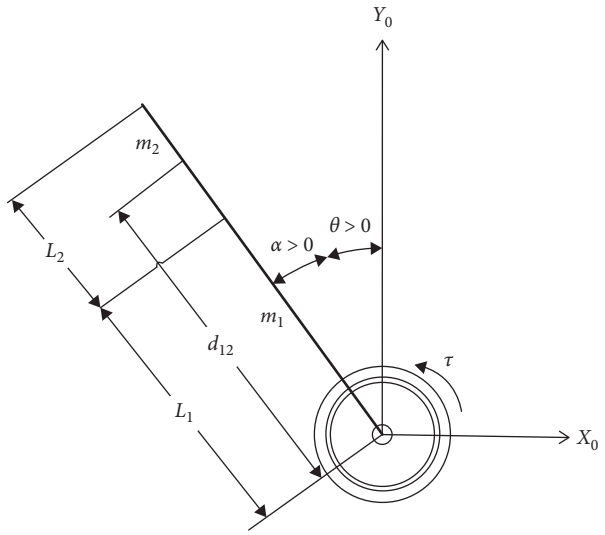

Figure 2: Schematic diagram of rotary flexible joint.

of the torque applied at the base of the rotary arm is described as follows:

$$\tau = \frac{k_t K_g \eta_m \eta_g \left(V_m - K_g k_m \dot{\theta}\right)}{R_m}, \tag{2}$$

where k_t is the motor torque constant, K_g is the gear ratio, the efficiency of motor and gearbox is symbolised by η_g and η_m, respectively, V_m is the controlled voltage, k_m is the motor's back-emf constant, and R_m represents the armature resistance.

The system dynamics of RFJ in the form of the state-space model are expressed by

$$\begin{aligned} \dot{\mathbf{x}} &= \mathscr{F}\mathbf{x} + \mathscr{G}V_m, \\ \mathbf{y} &= \mathscr{C}\mathbf{x} + \mathscr{D}V_m, \end{aligned} \tag{3}$$

where

$$\mathbf{x} = \begin{bmatrix} \theta & \alpha & \dot{\theta} & \dot{\alpha} \end{bmatrix}^T, \tag{4}$$

$$\mathscr{F} = \begin{bmatrix} 0 & 0 & 1 & 0 \\ 0 & 0 & 0 & 1 \\ 0 & \dfrac{K_s + B_l}{J_{\text{eq}}} & -\dfrac{B_{\text{eq}}}{J_{\text{eq}}} & \dfrac{B_l}{J_{\text{eq}}} \\ 0 & -\dfrac{(K_s + B_l)(J_l + J_{\text{eq}})}{J_l J_{\text{eq}}} & +\dfrac{B_{\text{eq}}}{J_{\text{eq}}} & -\dfrac{B_l(J_l + J_{\text{eq}})}{J_l J_{\text{eq}}} \end{bmatrix}, \tag{5}$$

$$\mathscr{G} = \begin{bmatrix} 0 & 0 & \dfrac{1}{J_{\text{eq}}} & -\dfrac{1}{J_{\text{eq}}} \end{bmatrix}^T, \tag{6}$$

$$\begin{aligned} \mathscr{C} &= \begin{bmatrix} 0 & 1 & 0 & 0 \end{bmatrix}, \\ \mathscr{D} &= \begin{bmatrix} 0 \end{bmatrix}. \end{aligned} \tag{7}$$

Several investigations are conducted to solve this issue as presented in Section 1. In this paper, the design problem is solved by implementing RCD controller to control and stabilize the RFJ system along with the motivation to compare its performance over other control strategies that include SMC and FOC.

3. Design of Robust and Converse Dynamic Controller

This section will illustrate the design methodology and implementation of RCD control for angular tracking and vibration control of flexible joint manipulator. The design methodology of RCD control is based on solving the inverse dynamics problem by engaging the non-square (pseudo) inversion. In RCD control, dynamic constraints in the form of differential equation are established that contains the control requirements. The equivalent or baseline control is derived by inverting the prescribed constraint dynamics along the trajectories of the dynamical system using the MPGI. The robust characteristics of RCD control are enhanced by augmenting SMC-based discontinuous (switching) control to cater modeling and parametric uncertainties and external disturbances.

3.1. Establishment of Constraint Equation. For tracking the horizontal arm angular position θ while suppressing the vibration angle α of the flexible joint, two constraint differential equations are formulated as a linear combination of the state deviation functions, whose order is equivalent to the relative degree of the controlled state variables, which implies

$$\ddot{\varrho}_\theta + c_1\dot{\varrho}_\theta + c_2\varrho_\theta = 0, \tag{8}$$

$$\ddot{\varrho}_\alpha + c_3\dot{\varrho}_\alpha + c_4\varrho_\alpha = 0, \tag{9}$$

where $\varrho_\theta = \theta - \theta_d$ and $\varrho_\alpha = \alpha - \alpha_d$ represent the state deviation functions. The coefficients appearing in the constraint differential equations, i.e., c_1, c_2, c_3, and c_4, are positive constant such that it will assure asymptotic stability of the two constraint equations given by (8) and (9). By Now, substitute the first and second time derivatives of the state deviation functions, i.e., $\varrho_{\dot{\theta}} = \dot{\theta} - \dot{\theta}_d$, $\varrho_{\dot{\alpha}} = \dot{\alpha} - \dot{\alpha}_d$, $\varrho_{\ddot{\theta}} = \ddot{\theta} - \ddot{\theta}_d$ and $\varrho_{\ddot{\alpha}} = \ddot{\alpha} - \ddot{\alpha}_d$ in the constraint differential equations given by (8) and (9) and solve for the controlled voltage V_m. This produces the following algebraic equations:

$$\begin{aligned} \frac{1}{J_{\text{eq}}}V_m &= \ddot{\theta}_d - m_{\dot{\theta}} - c_1\dot{\varrho}_\theta - c_2\varrho_\theta, \\ -\frac{1}{J_{\text{eq}}}V_m &= \ddot{\alpha}_d - m_{\dot{\alpha}} - c_3\dot{\varrho}_\alpha - c_4\varrho_\alpha, \end{aligned} \tag{10}$$

where c_1, c_2, c_3, and c_4 are positive real-valued constants. The algebraic equations stated above are prescribed in the form of state-space form, which implies

$$\begin{bmatrix} M_1 \\ M_2 \end{bmatrix} V_m = \begin{bmatrix} N_1 \\ N_2 \end{bmatrix}, \tag{11}$$

or

$$\mathscr{M}V_m = \mathscr{N}(\mathbf{x}, t), \tag{12}$$

where the vector elements of the control coefficient vector function $\mathscr{M}$: $\mathbb{R}^n \times [t_0, \infty) \longrightarrow \mathbb{R}^{2\times 1}$ are given as

$$\begin{aligned} M_1 &= \frac{1}{J_{\text{eq}}}, \\ M_2 &= -\frac{1}{J_{\text{eq}}}, \end{aligned} \tag{13}$$

and the vector elements of the control load function $\mathscr{N}(\mathbf{x}, t)$: $\mathbb{R}^n \times [t_0, \infty) \longrightarrow \mathbb{R}^{2\times 1}$ are inferred as

$$\begin{aligned} N_1 &= \ddot{\theta}_d - m_{\dot{\theta}} - c_1\dot{\varrho}_\theta - c_2\varrho_\theta, \\ N_2 &= \ddot{\alpha}_d - m_{\dot{\alpha}} - c_3\dot{\varrho}_\alpha - c_4\varrho_\alpha, \end{aligned} \tag{14}$$

where $m_{\dot{\theta}}$ and $m_{\dot{\alpha}}$ represent the third and fourth row elements of state transition matrix A given by (5) and are expressed as

$$\begin{aligned} m_{\dot{\theta}} &= \left[0 \quad \frac{K_s + B_l}{J_{\text{eq}}} \quad -\frac{B_{\text{eq}}}{J_{\text{eq}}} \quad \frac{B_l}{J_{\text{eq}}}\right]\mathbf{x}, \\ m_{\dot{\alpha}} &= \left[0 \quad -\frac{(K_s + B_l)(J_l + J_{\text{eq}})}{J_l J_{\text{eq}}} \quad +\frac{B_{\text{eq}}}{J_{\text{eq}}} \quad -\frac{B_l(J_l + J_{\text{eq}})}{J_l J_{\text{eq}}}\right]\mathbf{x}. \end{aligned} \tag{15}$$

3.2. Formulation of Baseline Inverse Control. The idea of baseline inverse (BI) control is to enforce the constraint dynamics given by (8) and (9) by generating the equivalent control voltage $V_{m_{\text{eq}}}$ such that the flexible arm tracks the joint angular position while dampening its vibrations. The baseline (equivalent) controlled voltage $V_{m_{\text{eq}}}$ is derived by engaging MPGI to find the inverse of the algebraic equation given by (11), which implies

$$V_{m_{\text{eq}}} = \mathscr{M}^{+}\mathscr{N}(\mathbf{x}, t), \tag{16}$$

where the notation $\mathscr{M}^{+}$ represents the MPGI of $\mathscr{M}$ described as

$$\mathscr{M}^{+} = \left\{\mathscr{M}^{T}\mathscr{M}\right\}^{-1}\mathscr{M}^{T}. \tag{17}$$

3.3. Augmentation of the Switching Control. The inclusion of the switching (discontinuous) term in the baseline controlled voltage $V_{m_{\text{eq}}}$ is inspired from the concept of conventional sliding mode theory [27]. The said augmentation will provide robust characteristics to counter parametric uncertainties, system nonlinearities, and bounded exogenous disturbances. In switching control, the sliding manifold vector function $\mathbf{s}$ is computed by taking the integral of the two constraint equations given by (8) and (9) and is presented as

$$\mathbf{s} = \begin{bmatrix} s_{\theta} \\ s_{\alpha} \end{bmatrix} = \begin{bmatrix} \dot{\varrho}_{\theta} + c_1\varrho_{\theta} + c_2\int \varrho_{\theta} \\ \dot{\varrho}_{\alpha} + c_3\varrho_{\alpha} + c_4\int \varrho_{\alpha} \end{bmatrix}. \tag{18}$$

Taking the time derivative of sliding vector function $\mathbf{s}$, we have

$$\dot{\mathrm{s}} = \begin{bmatrix} \ddot{\varrho}_{\theta} + c_1\dot{\varrho}_{\theta} + c_2\varrho_{\theta} \\ \ddot{\varrho}_{\alpha} + c_3\dot{\varrho}_{\alpha} + c_4\varrho_{\alpha} \end{bmatrix}, \tag{19}$$

or

$$\dot{\mathrm{s}} = \mathscr{M}V_m - \mathscr{N}(\mathbf{x}, t). \tag{20}$$

It is notable that the finite time convergence of $\mathbf{s}$ to zero implies the asymptotic realization of the constraint dynamics of θ and α given by (8) and (9), respectively, and its algebraic equivalence given by (11), by steering the trajectories of ϱ_{θ} and ϱ_{α} to their respective solution trajectories.

Based on the sliding surface vector, the switching control law is derived by using the principle of rate reaching law, which implies

$$V_{m_{sw}} = \mathscr{M}^{+}(\mathbf{x}, \nu, t)\mathscr{K}\frac{\mathbf{s}}{\|\mathbf{s}\|}, \tag{21}$$

where $\mathscr{K}$ is 2×2 positive definite diagonal matrix and $\|\cdot\|$ represents the Euclidean norm. The hybrid RCD controller expression which is comprised of the baseline (equivalent) and switching controlled voltage is written as

$$V_m = \overbrace{\mathscr{M}^{+}(\mathbf{x}, \nu, t)\mathscr{N}(\mathbf{x}, t)}^{V_{m_{\text{eq}}}} \underbrace{- \mathscr{M}^{+}(\mathbf{x}, \nu, t)\mathscr{K}\frac{\mathbf{s}}{\|\mathbf{s}\|}}_{V_{m_{sw}}}. \tag{22}$$

4. Stability Analysis

The stability analysis of the derived RCD control expression given by (22) is demonstrated using Lyapunov stability criterion. The finite time convergence of ϱ_{θ} and ϱ_{α} to zero is assured by suitable selection of the gain matrix $\mathscr{K}$. To prove this convergence, substitute the expression of V_m given by (22) in the sliding mode dynamics given by (20), which yields the following expression:

$$\begin{aligned} \dot{s} &= \mathscr{M}\left\{\mathscr{M}^{+}(\mathbf{x}, \nu, t)\mathscr{N}(\mathbf{x}, t) - \mathscr{M}^{+}(\mathbf{x}, \nu, t)\mathscr{K}\frac{\mathbf{s}}{\|\mathbf{s}\|}\right\} - \mathscr{N}(\mathbf{x}, t) \\ &= \left\{\mathscr{M}\mathscr{M}^{+} - \mathscr{I}_{2\times 2}\right\}\mathscr{N}(\mathbf{x}, t) - \mathscr{M}\mathscr{M}^{+}\mathscr{K}\frac{\mathbf{s}}{\|\mathbf{s}\|}. \end{aligned} \tag{23}$$

To demonstrate the finite time convergence of the sliding mode dynamics $\dot{s}$ given by (23) to zero, which implies the asymptotic realization of the constraint dynamics given by (8) and (9) and its algebraic equivalence given by (12), the following quadratic positive definite Lyapunov energy function is considered:

$$V = \frac{1}{2}\mathbf{s}^{T}\mathbf{s}. \tag{24}$$

The time derivative of Lyapunov function V is computed as

$$\begin{aligned} \dot{V} = \mathbf{s}^{T}\dot{\mathrm{s}} &= \mathbf{s}^{T}\left\{\left(\mathscr{M}\mathscr{M}^{+} - I_{2\times 2}\right)\mathscr{N}(\mathbf{x}, t) - \mathscr{M}\mathscr{M}^{+}\mathscr{K}\frac{\mathbf{s}}{\|\mathbf{s}\|}\right\} \\ &= \mathbf{s}^{T}\left(I_{2\times 2} - I_{2\times 2}\right)\mathscr{N}(\mathbf{x}, t) - \mathbf{s}^{T}\mathscr{M}\mathscr{M}^{+}\mathscr{K}\frac{\mathbf{s}}{\|\mathbf{s}\|}. \end{aligned} \tag{25}$$

The 2-(induced) norm of $\mathscr{M}\mathscr{M}^{+}$ is unity, and it follows that $\dot{V} \leq 0$ is guaranteed if the minimum singular value function $\sigma_{\min}(\mathscr{K}) > \|\mathscr{N}(\mathbf{x}(0), 0)\|$. Moreover, because $\dot{V} = 0$ occurs only at $\mathbf{s} = 0_2$, it follows from LaSalle's principle [28] that $\mathbf{s} = 0_2$ is attractive. Furthermore, the discontinuous term on the right hand side of (25) implies that this condition on $\mathscr{K}$ satisfies the finite time convergence of $\mathbf{s}$ and $\dot{s}$ to the zero vectors. The finite time convergence of $\mathbf{s}$ and $\dot{s}$ to zero will eventually guarantee the asymptotic convergence of ϱ_{θ} and ϱ_{α} to zero. It is assumed that for any given initial state condition, the stability condition is satisfied by arbitrarily increasing the gain matrix $\mathscr{K}$, which implies the semiglobal asymptotic stability of the errors ϱ_{θ} and ϱ_{α} to zero.

5. Numerical Simulation and Experimental Investigation

In this section, computer simulations and experiments are used to verify the performance of RCD control law for the flexible manipulator, in which the angular commands can be obtained while simultaneously suppressing the oscillations. During simulations and experiments, the manipulator system is assumed to be initially situated at the following conditions: $\mathbf{x}_i = [0000]^{T}$.

5.1. Numerical Simulation. To assess the tracking abilities of RCDs, numerical simulations are performed to examine their dynamic characteristics. Square-wave profiles of

±20 deg amplitude and 0.33 Hz frequency are used to command the flexible manipulator's angular trajectory. Table 1 also accounts for the parametric variations of 20% when calculating the numerical values of the flexible joint system.

Furthermore, the performance of RCD control is compared with the conventional baseline inverse (BI) control approach which is basically a baseline or equivalent control given by (16) to demonstrate the superiority of the discontinuous switching term. The numerical values of the RCD control parameters are set to be $c_1 = 701.5, c_2 = 2946, c_3 = 335.1, c_4 = 7152.6, k_1 = 140$, and $k_2 = 0.1$, where k_1 and k_1 are diagonal elements of 2×2 sliding mode gain matrix $\mathscr{K}$. The closed-loop response of the joint angle θ and the vibration angle α for a square-wave profile is shown in Figures 3 and 4. The RCD control demonstrates better control performance with much smaller tracking error as compared to the conventional BI control strategy because of the convergence and robustness attributes of the SMC-based discontinuous control term. The response curve of joint angle θ is much faster with RCD as compared to BI control as shown in Figure 3. This faster convergence of joint angle θ will be responsible to excite bigger variation in vibration angle α. Additionally, the key performance indices of RCD and baseline inverse (BI) control methodologies in response to the square-wave input are listed in Table 2. The time histories of the controlled voltage input to the joint angle V_m are shown in Figure 5, which are very much realizable.

5.2. Experimental Results. Experimental investigation of RCD control is conducted on Quanser's flexible joint manipulator system to demonstrate its practical applicability. There is a base module, a horizontal rotary arm, and two springs in the experimental setup. Figure 6 shows the hardware setup required for performing the experiments.

(1) Voltage module (Quanser VoltPAQ).

(2) An organization that collects data (Quanser Q8-USB, QPID/QPIDe).

(3) Specialty plants in hover (Quanser hover).

(4) Control software in real time (QUARC-Simulink configuration).

RCD control expression consists of two components in experimental setup, i.e., $V_{m_{eq}}$ and $V_{m_{eq}}$ given by (22) are implemented in Matlab Simulink environment. QUARC (Quanser Real-Time Control) is used to interact with RFJ hardware via Simulink. QUARC can be easily configured with Simulink environment to provide simulation model execution in real time on a variety of targets, allowing Simulink models to be accelerated. Data are fed from the horizontal arm and flexible joint from the RFJ test bench to the Simulink module using the Q8-USB data acquisition board. For the following two scenarios, we kept the same RCD control design parameters for experimental investigation as we did for computer simulations.

Table 1: RFJ system specifications.

Parameters	Nominal value	Perturbed value
B_{eq} (N.m/(rad/s))	0.004	0.0048
J_{eq} (kg m^3)	2.08×10^{-3}	2.49×10^{-3}
m_1 (kg)	0.064	0.076
m_2 (kg)	0.03	0.036
L_1 (m)	0.298	0.357
L_2 (m)	0.156	0.187

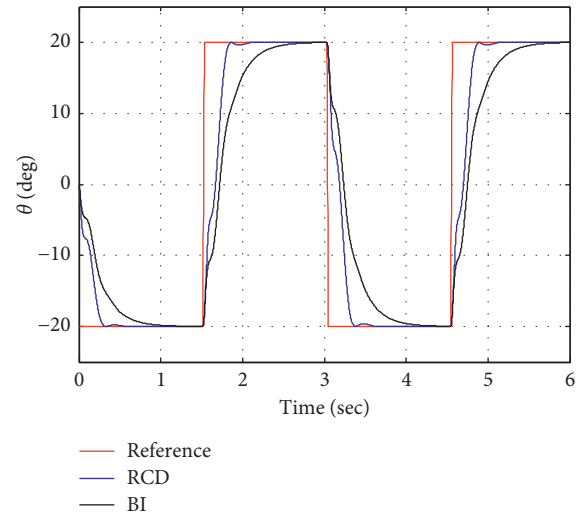

Figure 3: Joint angle vs. time.

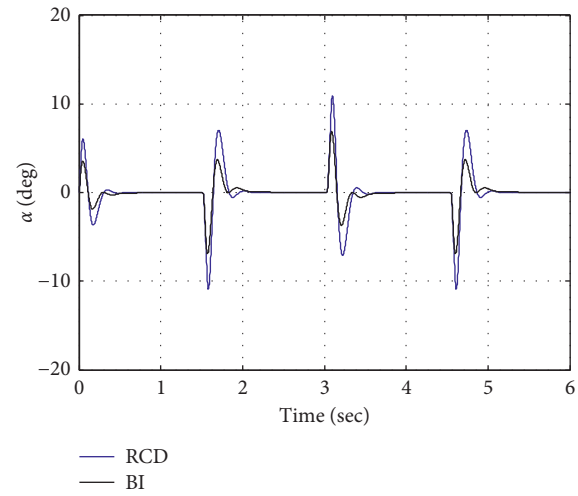

Figure 4: Vibration angle vs. time.

Table 2: Key performance indices of RCD and BI control schemes.

Parameters (sec)	RCD	BI scheme
Rise time	0.2	0.28
Settling time	0.55	1.3

5.2.1. Square-Wave Tracking. To the horizontal rotary arm, a square-wave profile with an amplitude of ±20 deg and a frequency of 0.1 Hz is used as an input parameter. The results

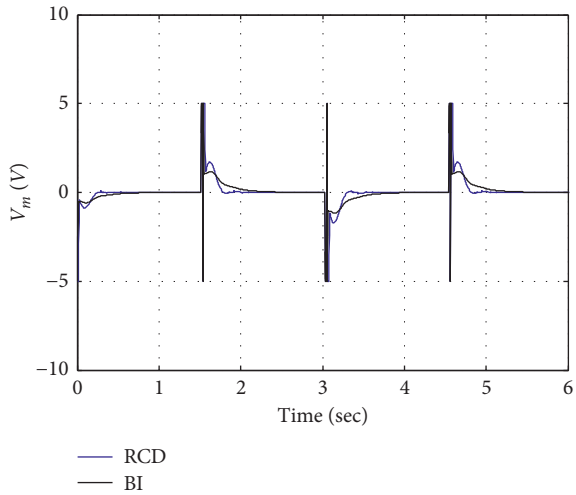

Figure 5: Controlled voltage vs. time.

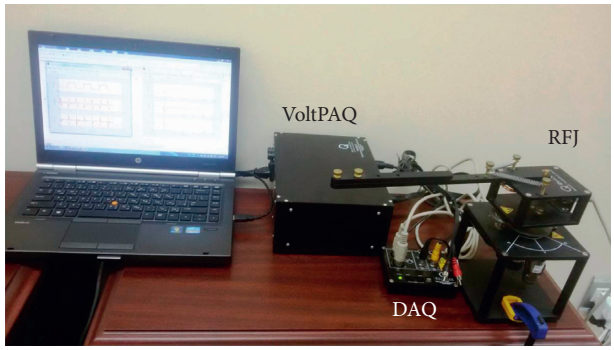

Figure 6: Experimental setup.

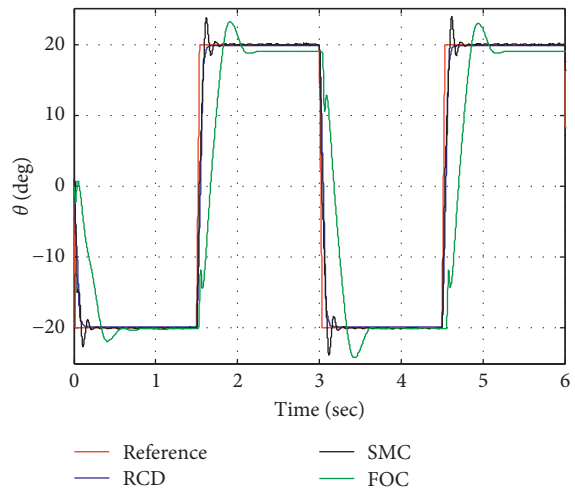

Figure 7: Experimental results: arm angle vs. time.

of RCD control are also compared with classical SMC, FOC, and traditional baseline (equivalent) BI control strategies. As shown in Figures 7 and 8, the experiment aims to track the joint oscillations of a manipulator while damping them.

The RCD-based tracking response is superior in terms of the rise time, settling time, and less overshoot as compared

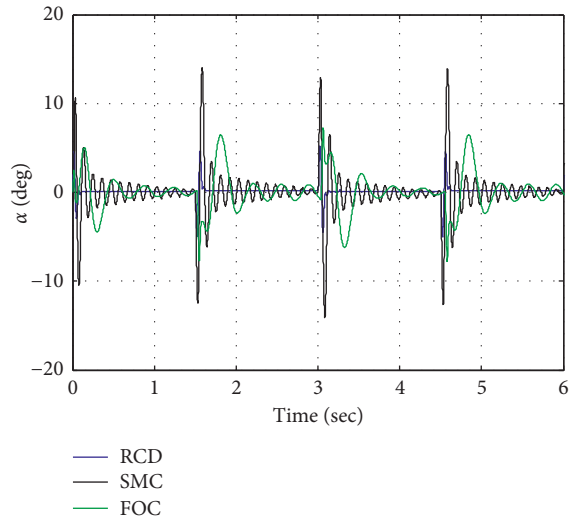

Figure 8: Experimental results: joint angle vs. time.

Table 3: Comparative analysis.

Parameters	RCD	SMC	FOC	BI
Rise time (sec)	0.08	0.08	0.28	0.19
Settling time (sec)	0.154	0.29	0.63	0.28
Overshoot (%)	0	11.9	11.6	0

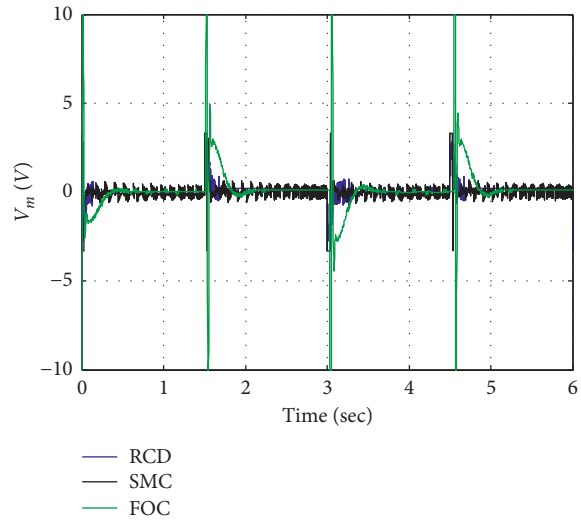

Figure 9: Experimental results: controlled voltage vs. time.

with SMC, FOC, and BI approaches. The performance indices of the transient behaviour are listed in Table 3.

The corresponding control voltages are shown in Figure 9 which are well under saturation limit.

5.2.2. Disturbance Rejection. As part of this experiment, manual disturbances are applied to the system at different instantaneous times to analyze its robustness. To see how efficiently the controller rejects the applied disturbance while

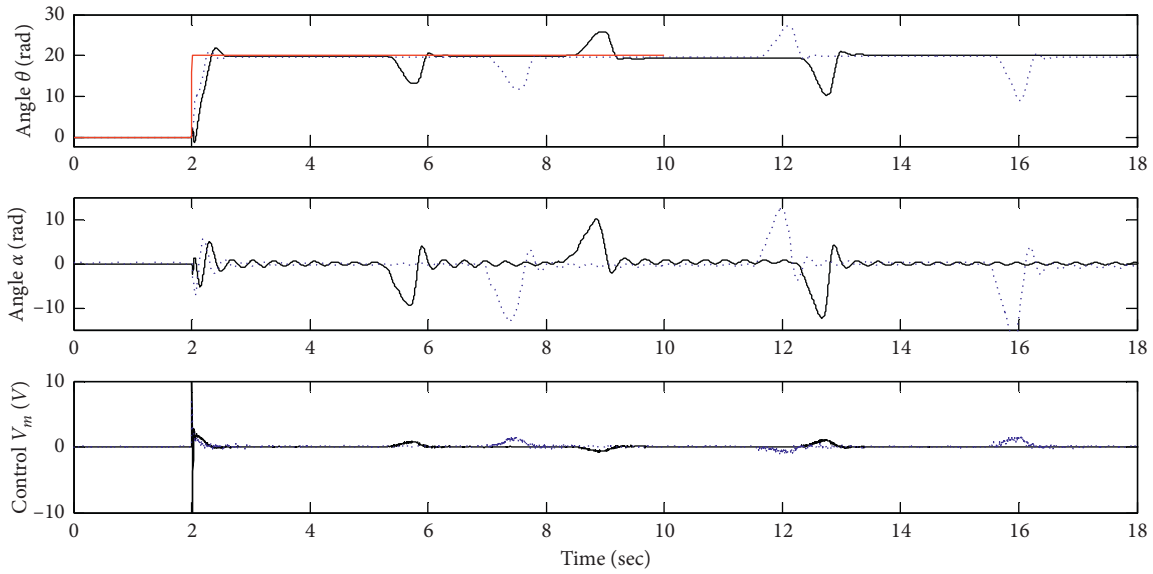

Figure 10: Disturbance rejection experimental results (solid line: RCD controller; dashed line: traditional SMC scheme).

suppressing vibrations, a light tap is applied to the horizontal rotary arm. The reference inputs to the rotary arm are a step command of ±1 deg. As shown in Figure 10, the proposed controller incorporates an angle command to the rotary arm, while keeping the oscillations of the joint subjected to disturbances to a minimum. Experimental results show that the controlled voltage V_m is observed within the limits of the Figure 10 result, thereby ensuring the control power is acceptable.

6. Conclusion

In this paper, RFJ manipulator system end-point tracking control is demonstrated using RCD control. Integrating discontinuous elements with BI can improve the closed-loop performance even in the presence of parameters that are uncertain and perturbed. Experimentally and numerically, the RCD control scheme is evaluated and tested to demonstrate its robustness beyond simply tracking the position of the joint. In experimentation, RCD is compared with conventional SMC and FOC control strategies to evaluate how well each control strategy handles disturbances and nonlinearities for accurate, desirable, and superior tracking performance.

Data Availability

No data were used to support this study.

Conflicts of Interest

The authors declare that they have no conflicts of interest.

Acknowledgments

This project was funded by the Deanship of Scientific Research (DSR) at King Abdulaziz University, Jeddah, under grant no. G: 190-135-1441. The authors, therefore, acknowledge with thanks DSR for technical and financial support.

References

[1] J. Daafouz, G. Garcia, and J. Bernussou, "Robust control of a flexible robot arm using the quadratic d-stability approach," *IEEE Transactions on Control Systems Technology*, vol. 6, no. 4, pp. 524–533, 1998.

[2] V. Feliu, K. S. Rattan, and H. B. Brown, "Modeling and control of single link flexible arms with lumped masses," *Journal of Dynamic Systems, Measurement, and Control, Transactions of the ASME*, vol. 114, no. 59, pp. 59–69, 1992.

[3] J. Jalani and S. Jayaraman, "Design a fuzzy logic controller for a rotary flexible joint robotic arm," *Malaysia Technical Universities Conference on Engineering and Technology*, vol. 150, pp. 1–6, 2018.

[4] A. Chatterjee, R. Chatterjee, F. Matsuno, and T. Endo, "Augmented stable fuzzy control for flexible robotic arm using LMI approach and neuro-fuzzy state space modeling," *IEEE Transactions on Industrial Electronics*, vol. 55, no. 3, pp. 1256–1270, 2008.

[5] D. H. Kim and W. H. Oh, "Robust control design for flexible joint manipulators: theory and experimental verification," *International Journal of Control, Automation, and Systems*, vol. 4, pp. 495–505, 2006.

[6] S. Seiji, D. Mingcong, I. Akira, and J. Changan, "Vibration control of a flexible arm experimental system with hysteresis of piezoelectric actuator," *International Journal of Innovative Computing, Information and Control*, vol. 6, pp. 2965–2975, 2010.

[7] M. A. Auwalu, Z. Mohamed, M. Mustapha, and A. Bature, "Vibration and tip deflection control of a single link flexible manipulator," *International Journal of Instrumentation and Control Systems*, vol. 3, no. 4, pp. 17–27, 2013.

[8] E. Pereira, S. S. Aphale, V. Feliu, and S. O. R. Moheimani, "Integral resonant control for vibration damping and precise tip-positioning of a single-link flexible manipulator," *IEEE/ASME Transactions on Mechatronics*, vol. 16, no. 2, pp. 232–240, 2011.

[9] W. Wei Yen, C. Yi Hsing, and L. Tsu Tian, "Observer based fuzzy control for a class of general nonaffine nonlinear systems using generalized projection update laws," *IEEE Transactions on Fuzzy Systems*, vol. 19, no. 3, pp. 493–504, 2011.

[10] Y. Li, S. Tong, and T. Li, "Adaptive fuzzy output feedback control for a single-link flexible robot manipulator driven DC motor via backstepping," *Nonlinear Analysis: Real World Applications*, vol. 14, no. 1, pp. 483–494, 2013.

[11] D. H. Kim, "Control desing for flexible joint manipulators with mismatched uncertainty: adaptive robust scheme," *Transaction on Control, Automation, and Systems*, vol. 1, no. 1, pp. 32–43, 1999.

[12] U. M. Al-Saggaf, I. M. Mehedi, R. Mansouri, and M. Bettayeb, "State feedback with fractional integral control design based on the Bode's ideal transfer function," *International Journal of Systems Science*, vol. 47, no. 1, pp. 149–161, 2016.

[13] I. M. Mehedi, "State feedback based fractional order control scheme for linear servo cart system," *Journal of Vibroengineering*, vol. 20, no. 1, pp. 782–792, 2018.

[14] M. Bettayeb, R. Mansouri, U. Al-Saggaf, and I. M. Mehedi, "Smith predictor based fractional-order-filter PID controllers design for long time delay systems," *Asian Journal of Control*, vol. 19, no. 2, pp. 587–598, 2016.

[15] I. M. Mehedi, U. M. Al-Saggaf, R. Mansouri, and M. Bettayeb, "Stabilization of a double inverted rotary pendulum through fractional order integral control scheme," *International Journal of Advanced Robotic Systems*, vol. 16, no. 4, pp. 1–9, 2019.

[16] I. M. Mehedi, U. M. Al-Saggaf, R. Mansouri, and M. Bettayeb, "Two degrees of freedom fractional controller design: application to the ball and beam system," *Measurement*, vol. 135, pp. 13–22, 2019.

[17] U. M. Al-Saggaf, I. M. Mehedi, R. Mansouri, and M. Bettayeb, "Rotary flexible joint control by fractional order controllers," *International Journal of Control, Automation and Systems*, vol. 15, no. 6, pp. 2561–2569, 2017.

[18] Z. Li, H. Yan, H. Zhang, J. Sun, and H. K. Lam, "Stability and stabilization with additive freedom for delayed takagi-sugeno fuzzy systems by intermediary polynomial-based functions," *IEEE Transactions on Fuzzy Systems*, vol. 28, no. 4, pp. 692–705, 2019.

[19] Z. Li, H. Yan, H. Zhang, J. Sun, and C. Huang, "Stability analysis for delayed neural networks via improved auxiliary polynomial-based functions," *IEEE Transactions on Neural Networks and Learning Systems*, vol. 30, no. 8, pp. 2562–2568, 2018.

[20] D. Singh, V. Kumar, V. Yadav, and M. Kaur, "Deep neural network-based screening model for COVID-19-infected patients using chest X-ray images," *International Journal of Pattern Recognition and Artificial Intelligence*, vol. 35, no. 3, Article ID 2151004, 2021.

[21] M. Kaur, V. Kumar, V. Yadav, D. Singh, N. Kumar, and N. N. Das, "Metaheuristic-based deep COVID-19 screening model from chest X-ray images," *Journal of Healthcare Engineering*, vol. 2021, Article ID 8829829, 9 pages, 2021.

[22] I. M. Mehedi, U. Ansari, and U. M. Al-Saggaf, "Three degrees of freedom rotary double inverted pendulum stabilization by using robust generalized dynamic inversion control: design and experiments," *Journal of Vibration and Control*, vol. 26, no. 23-24, pp. 2174–2184, 2020.

[23] L. Zhichen, Y. Huaicheng, Z. Hao, Z. Xisheng, and H. Congzhi, "Improved inequality-based functions approach for stability analysis of time delay system," *Automatica*, vol. 108, Article ID 108416, 2019.

[24] Z. Li, H. Yan, H. Zhang, Y. Peng, J. H. Park, and Y. He, "Stability analysis of linear systems with time-varying delay via intermediate polynomial-based functions," *Automatica*, vol. 113, Article ID 108756, 2020.

[25] Quanser Inc, *Rotary Flexible Joint-Workbook*, Quanser Inc, Markham, Ontario, Canada, 2011, http://my.nps.edu/documents/105873337/0/Flexible+Joint+ Workbook+_ Instructor_.pdf/c4d53197-cc41-4cb4-bb2e-a88008529749.

[26] Quanser Inc, *Quanser SRV02 User Manual*, Quanser Inc, Markham, Ontario, Canada, 2009.

[27] J. Liu and X. Wang, *Advanced Sliding Mode Control for Mechanical Systems*, Springer, Berlin, Germany, 2012.

[28] H. K. Khalil, *Noninear Systems*, Prentice-Hall, Hoboken, NJ, USA, 1996.